Scientific Research Publishing

Journal of High Energy Physics, Gravitation and Cosmology, 2026, 12(3), 1741-1758
https://www.scirp.org/journal/jhepgc
ISSN Online: 2380-4335
ISSN Print: 2380-4327

Fits to All 175 SPARC Galaxies with the Graviton Redshift Theory of Dark Matter

Firmin J. Oliveira

East Asian Observatory/James Clerk Maxwell Submillimetre Telescope, Hilo, HI, USA
Email: firmjay@hotmail.com

How to cite this paper: Oliveira, F.J. (2026) Fits to All 175 SPARC Galaxies with the Graviton Redshift Theory of Dark Matter. *Journal of High Energy Physics, Gravitation and Cosmology*, **12**, 1741-1758.
https://doi.org/10.4236/jhepgc.2026.123089

Received: April 4, 2026
Accepted: July 20, 2026
Published: July 23, 2026

Abstract

The graviton redshift theory (GRST) is the theory that gravitons lose energy thru gravitational redshift while traveling in the accelerating system of a gravitational field. In this report, we show that the GRST when applied to the galaxies in the Spitzer Photometry and Accurate Rotation Curves database gives reasonable fits to the rotation curves of all 175 galaxies in the database using a fixed set of parameters. Three basic parameters are involved: the baryonic Tully-Fisher relation normalization multiplier A_{gal}, the coupling constant scale k and the coupling constant exponent β. In the fitting process for all the galaxies, the tables of values for the parameters are pre-defined at the beginning, using a working set of parameter values obtained during preliminary trials, and then these values are not altered during the entire fitting procedure. The emphasis of this report will be to critique the GRST by the analysis of the fits made in terms of the distributions of masses, coupling constants and fitting errors.

Keywords

Spiral Galaxies, Dark Matter, Gravitons, Gravitational Redshift, Baryon Mass Densities

1. Introduction

This is a report on the application of the graviton redshift theory (GRST) [1], which is the theory that gravitons lose energy thru gravitational redshift while traveling in the accelerating system of a gravitational field. Accessing the Spitzer Photometry and Accurate Rotation Curves (SPARC) database, we give the results of fits to all 175 galaxies using a fixed set of parameters. What we are given from the SPARC database are the observed galaxy rotation radial positions and velocities. Also given are the velocity profiles representing the mass-to-light ratios for the rotation disk and bulge of the galaxy and the velocity profile for the Hydrogen (H-I) and Helium (He) gas in the galaxy. We are given other observables such as the distance to the galaxy and some photometry which we do not use here. We assume that there are only baryons in the galaxy which emit light from the stars and radio emissions from the gases. We assume the existence of gravitons which transfer the force of the gravitational field due to the mass of the baryons. Given an estimate of the total galaxy baryonic mass and assuming that the disk and bulge mass-to-light ratios are constant and proportional, we can determine a mass-to-light ratio Υ_* for the stars. What is seen in galaxy observations is that the actual rotational velocities are very often greater than the Newtonian velocities due to only the baryons especially in the outer galaxy positions, for which non-baryonic dark matter has been hypothesized. Thus, we seek a model to account for the observed rotation velocities of any spiral or dwarf galaxy based on only baryons and the gravitons hypothesized to be associated with them. We propose that the effect traditionally attributed to unknown particles of dark matter can be fulfilled by the gravitational redshift of the gravitons.

First off, we need to determine a value for the total baryonic mass for a SPARC galaxy [2]. This is just a pure guess but we can base it on the baryonic Tully-Fisher relation (BTFR) [3] [4] since this has been used to fit many galaxies and especially for the SPARC galaxies which we will access exclusively in this report. So, we say that the total baryonic mass in solar units $\mathrm{M}_\odot$ for a galaxy is given by $M_{bgal}/\mathrm{M}_\odot = A_{gal} 50\left(v_f\right)^4$ for some dimensionless multiple A_{gal} with v_f the final velocity observed for the galaxy. Next, since we assume that gravitons exist and that they travel at constant speed c in the galaxy, the same as the speed of light, then the gravitons will experience a lessening of their energy due to the gravitational redshift phenomenon, which is essentially a gravitational time speed up effect at lesser gravitational field strengths farther away from the center of the galaxy mass. This energy loss can be accounted as a mass loss using Einstein's relation $\delta\{\text{mass}\} = \delta\{\text{energy}\}/c^2$. We provide a specific form of how this energy couples into the gravitational field to deliver the observed results of the rotations of stars and gas, which is expressed in the form,

$$\begin{aligned}
\Delta\{\text{Energy}\}(r) &= K(r;k,\beta)\int_0^v \left(mc^2\right)\frac{\delta v}{c} \\
&= K(r;k,\beta)\int_0^t (mc)\,a(t)\,\delta t \\
&= -K(r;k,\beta)\int_0^r \left(m\frac{GM_b(s)}{s^2}\right)\mathrm{d}s,
\end{aligned} \tag{1}$$

where $K(r;k,\beta)$ is a coupling function which has two constant coupling parameters k and β, m is the orbiting test mass, $\delta v = a(t)\delta t$ is the change in velocity of an observer in freefall along the way in the gravitational field with respect to an observer in an inertial system at a large distance from the galaxy, $\delta t = \delta r/c$ is the short travel time of the gravitons at speed c over distance δr. The acceleration a at a point r in the field is given by

$a(r(t)) = -GM_b(r)/r^2$ and the integral is the sum of the work done by the system as the gravitons travel from the inner galaxy to the orbiting mass. We assume that $K(r;k,\beta)$ takes the form,

$$K(r;k,\beta) = k\left(\frac{r_f}{r}\right)^{\beta} \frac{M_b(r)}{M_b(r_f)}, \tag{2}$$

where k and β are coupling constants, $M_b(r)$ is the baryon mass at radial position r and $M_b(r_f) = M_{bgal}$ is the total baryon mass of the galaxy at the final galaxy radial position r_f.

Just applying Newton's laws using the baryonic mass to obtain the rotational velocities falls short of the observed rotational velocities in most cases. To fix this, since we think that the gravitational redshift energy loss of the gravitons can provide the necessary missing mass, then, using (1) and (2), our function for the rotational velocity of an orbiting mass takes the form,

$$\begin{aligned} v^2(r;k,\beta) &= \frac{GM_b(r)}{r} + K(r;k,\beta)\int_0^r \left(\frac{GM_b(s)}{s^2}\right)\mathrm{d}s \\ &= \left(\frac{GM_b(r)}{r}\right)\left(1 + k\left(\frac{r_f}{r}\right)^{\beta}\left(\frac{r}{M_b(r_f)}\right)\int_0^r\left(\frac{M_b(s)}{s^2}\right)\mathrm{d}s\right). \end{aligned} \tag{3}$$

From the second equation of (3), we can obtain a value for the coupling constant k at the final position r_f since the factor $(r_f/r)^{\beta} = 1$ for $r = r_f$, this yields,

$$k = \frac{\left(v_f^2 - \dfrac{GM_b(r_f)}{r_f}\right)}{\left(\displaystyle\int_0^{r_f}\left(\frac{GM_b(u)}{u^2}\right)\mathrm{d}u\right)}. \tag{4}$$

With the value obtained for k then the constant β can be determined by minimizing the error of the fit of the predicted rotation curve for $v^2(r;k,\beta)$ given by (3) to the observed rotation curve $v_{obs}^2(r)$. This is expressed by the general form,

$$\beta = \beta_{min} \text{ where } \left(\left|v_{obs}^2(r) - v^2(r;k,\beta_{min})\right|\right) = \text{minimum}\left(\left|v_{obs}^2(r) - v^2(r;k,\beta_x)\right|\right), \tag{5}$$

for a sequence of β_x. Subsequently, we will explain the algorithm to setup the lists of parameter values for A_{gal}, k and β. Additionally, there are also the mass-to-light ratio parameters Υ_{dsk} and Υ_{bul} obtained from the mass and velocity profiles for the stars in the disk and bulge, respectively, of the galaxy data.

2. Algorithms for Determining the Baryon Mass, Mass-to-Light Ratios and Coupling Constants

The values for A_{gal} are taken from a list of N_A elements defined by,

$$A_{gal} \in \left\{A_{j-1} + dA,\ j = 1,2,\cdots,N_A - 1, A_0 = 0.01, dA = 40/(N_A - 1), N_A = 152\right\}. \tag{6}$$

This gives the 152 list values of $\{0.01, 0.275, 0.54, \cdots, 39.48, 39.745, 40.01\}$. To obtain the galaxy mass for a particular instance j of the fitting process with normalization multiplier $A_{gal,j}$, and the final observed galaxy velocity v_f, the total baryonic mass $M_{bgal,j}$ for the instance is given by,

$$M_{bgal,j} = A_{gal,j} 50 \left(v_f\right)^4 \mathrm{M}_{\odot}. \tag{7}$$

The values for coupling constant k are taken from a list of N_k elements defined by,

$$k \in \left\{ (i) dk, i = 0,1,\cdots, N_k - 1, dk = 0.08, N_k = 62 \right\}. \tag{8}$$

This gives the 62 list values for k of $\{0, 0.08, 0.16, \cdots, 4.72, 4.8, 4.88\}$.

The values for β are taken from a list of N_β elements defined by,

$$\beta \in \left\{ \beta_n = \beta_{n-1} + d\beta, n = 1,2,\cdots, N_\beta - 1, \beta_0 = -6, d\beta = 12/\left(N_\beta - 1\right), N_\beta = 62 \right\}. \tag{9}$$

This gives the 62 list values for β of $\{-6.0, -5.803, -5.607, \cdots, 5.607, 5.803, 6.0\}$. A constant mass-to-light ratio Υ_{dsk} is assumed for a galaxy disk and it is assumed that the galaxy bulge, if it exists, has a mass-to-light ratio proportional to that of the disk, namely $\Upsilon_{bul} = \left(bul_{fac}\right)\Upsilon_{dsk}$. Then, since the mass-to-light ratio is assumed constant, we can evaluate it at the final position r_f for each instance j of the baryonic mass $M_{bgal,j}$ obtained from (7), which is expressed by,

$$\Upsilon_{dsk,j} = \frac{\left(M_{bgal,j} G/r_f\right) - v_{gasf}\left|v_{gasf}\right|}{v_{dskf}\left|v_{dskf}\right| + \left(bul_{fac}\right) v_{bulf}\left|v_{bulf}\right|}, \tag{10}$$

where absolute values $||$ are needed because v_{gas} can sometimes be negative (Ref. [2], p. 5). For the fits we set $bul_{fac} = 1.4$ for all galaxies [2].

The algorithm for the fits performed in this case consists of selecting a possible total baryonic mass $M_{b,j}$ from (7), determine the mass-to-light ratios Υ_{dskj} and Υ_{bulj} using (10). From the photometric data which has been reduced to the equivalent velocities for the galaxy bulge, disk and gas mass content, we calculate instance j of the baryonic mass function $M_{b,j}(r)$ within radial distance r from the galaxy center as due to a spherically symmetric distribution using the Newtonian relation,

$$M_{b,j}(r) = \left(\frac{r}{G}\right)\left(\left(\left|v_{gas}(r)\right| v_{gas}(r)\right) + \Upsilon_{dsk,j}\left(\left|v_{dsk}(r)\right| v_{dsk}(r)\right) + \Upsilon_{bul,j}\left(\left|v_{bul}(r)\right| v_{bul}(r)\right)\right), \tag{11}$$

where $r = r_k$, $k = 0,1,\cdots, N_{obs} - 1$, where N_{obs} is the number of radial distances observed, and the absolute values of the velocities are needed because they can sometimes be negative (Ref. [2], p. 5). The baryon mass profile velocities for the disk, bulge and gas are taken from Table2.mrt of the SPARC database.

With the total baryon mass for the instance j being $M_{b,j}\left(r_f\right) = M_{bgal,j}$ at the last galaxy radial position r_f, since for $r = r_f$ the value of $\left(r_f/r\right)^\beta = 1$, a value for the constant coupling scale k is determined at the final radial position. By determining for each instance of the theoretical circular rotation velocity $v_{j,i}(r)$ for instance j computed at the final radial position $r = r_f$ with each of the possible instances of k_i from the list (12) and determining the error with the observed final velocity $v_{obs}(r_f)$, given by,

$$k_{err,j,i} = \frac{\left(v_{obs}(r_f)\right)^2 - \left(GM_{b,j}(r_f)/r_f + (k_i)\int_0^{r_f}\left(GM_{b,j}(s)/s^2\right)\mathrm{d}s\right)}{\int_0^{r_f}\left(GM_{bj}(s)/s^2\right)\mathrm{d}s}, \tag{12}$$

where $i = 0,1,\cdots,N_k - 1$. After determining each error $k_{err,j,i}$ for the instance of mass $M_{b,j}$, the value of k_j for that instance is determined by the minimum error,

$$\begin{aligned} &k_j = k_{imin},\ \text{where}\left|k_{err,j,imin}\right| \le \left(\left|k_{err,j,i}\right| \text{ for } i, imin \in \{0,1,\cdots,N_k - 1\}\right), \\ &j \in \{0,1,\cdots,N_A - 1\}. \end{aligned} \tag{13}$$

Now having the mass distribution instances $M_{b,j}(r)$ and the coupling constant scale value k_j for each instance, the best coupling coefficient β_j can be determined by the minimum error between the observed galaxy rotation velocity $v_{obs}(r)$ and the theoretical velocity $v_{j,n}(r)$. The theoretical velocity has the form,

$$\begin{aligned} v_{j,n}^2(r) &= \frac{GM_{b,j}(r)}{r} + k_j\left(\frac{r_f}{r}\right)^{\beta_n}\left(\int_0^r \frac{GM_{b,j}(s)}{s^2}\mathrm{d}s\right), \\ &j \in \{0,1,\cdots,N_A - 1\}, \\ &n \in \{0,1,\cdots,N_\beta - 1\}. \end{aligned} \tag{14}$$

The error between the observed and theoretical rotation velocities is expressed,

$$v_{err,j,n} = \frac{1}{\left(v_f\right)^2 N_{obs}} \sum_{s=0}^{(N_{obs}-1)} \left(\left|\left(v_{obs}(r_s)\right)^2 - \left(v_{j,n}(r_s)\right)^2\right|\right). \tag{15}$$

The best value for the exponent β_j is determined by the minimum error,

$$\begin{aligned} &\beta_j = \beta_{nmin},\ \text{where}\left|v_{err,j,nmin}\right| \le \left(\left|v_{err,j,n}\right| \text{ for } n, nmin \in \{0,1,\cdots,N_\beta - 1\}\right), \\ &j \in \{0,1,\cdots,N_A - 1\}. \end{aligned} \tag{16}$$

Finally, the errors between the observed and theoretical velocities are determined using the instance values for the triplets $\left(M_{b,j}, k_j, \beta_j\right)$ and then the minimum of the errors gives the best triplet. To do this we use the observed $v_{obs}(r)$ and the theoretical $v_{j,j}(r)$ using (14), where the error is expressed by,

$$Err_j = \left(\frac{1}{N_{obs}\left(v_f\right)^2}\right) \sum_{s=0}^{(N_{obs}-1)} \left(\left|\left(v_{obs}(r_s)\right)^2 - \left(v_{j,j}(r_s)\right)^2\right|\right). \tag{17}$$

The best galaxy value for the triplet $\left(M_{bgal}, k, \beta\right)$ is determined by the minimum error of Err_j in (17), yielding instance $j = jmin$ for the triplet,

$$\left(M_{bgal}, k, \beta\right) = \left(M_{b,jmin}, k_{jmin}, \beta_{jmin}\right),\ \text{where}\left|Err_{jmin}\right| \le \left|Err_j\right| \text{ for } j, jmin \in \{0,1,\cdots,N_A - 1\}. \tag{18}$$

3. Results

We use the velocities from the SPARC database [2], derived from near-infrared surface photometry at 3.6 μm. To simplify the analysis, we set the mass-to-light ratios for the disk and bulge to be constant and proportional [2] where $\Upsilon_{bul} = (bul_{fac})\Upsilon_{dsk}$ with $bul_{fac} = 1.4$. From the photometric data which has been reduced to the equivalent velocities for the galaxy bulge, disk and gas mass content, we calculate the baryonic mass function $M_b(r)$ within radial distance r from the galaxy center as due to a spherically symmetric distribution using the Newtonian relation,

$$M_b(r) = \left(\frac{r}{G}\right)\left(\left(|v_{gas}(r)|v_{gas}(r)\right) + \Upsilon_{dsk}\left(|v_{dsk}(r)|v_{dsk}(r)\right) + (bul_{fac})\Upsilon_{dsk}\left(|v_{bul}(r)|v_{bul}(r)\right)\right), \quad (19)$$

where $r = r_n$, $n = 0,1,\cdots,N-1$, $N > 1$, N the number of radial distances observed, and the absolute values of the velocities are needed because they can sometimes be negative (Ref. [2], p. 5). The rotation curve observed velocities and the mass profile velocities for the disk, bulge and gas are taken from Table2.mrt of the SPARC database.

Using the SPARC results at radial distance r for the gas, disk and bulge velocities for the galaxy, where the mass internal to r is given by $M_b(r)$ of (19), we obtain the equivalent graviton energy loss using (3), where the graviton mass function $M_g(r)$ is given by,

$$M_g(r_n) = k\left(\frac{r_f}{r_n}\right)^{\beta}\left(\frac{M_b(r_n)}{M_{bgal}}\right)\left(\frac{r_n}{G}\right)\sum_{j=0}^{n}\left(\int_{r_{j-(j>0)}}^{r_j}\left(\frac{GM_b(u)}{u^2}\right)\mathrm{d}u\right), \quad (20)$$

where $n = 0,1,\cdots,N-1$. The predicted velocity (3) using (19) and (20) is expressed in the form,

$$v^2(r_n) = \frac{G\left(M_b(r_n) + M_g(r_n)\right)}{r_n}, \quad (21)$$

where $n = 0,1,\cdots,N-1$, $N > 1$. For clarity, in (20) the logical expression term $(j > 0)$ equals 1 if j is greater than 0, and zero otherwise. **Table 1** shows data used for all the 175 SPARC galaxy fits.

3.1. Parameters Used in Fits to the SPARC Galaxies

Figure 1 shows distribution plots. Plot (a) shows the distribution for the A_{gal} parameters, averaged by division by $Ndat = 175$. The Poisson distribution,

$$P(\lambda, x) = \frac{\lambda^x}{\Gamma(x+1)}\exp(-\lambda), \quad (22)$$

where λ is the expected rate of occurrence of an event in a given interval of A_{gal} space and x is the number of occurrences in that interval and $\Gamma(x)$ is the gamma function, where $\Gamma(n+1) = n!$ for integer n. For this analysis, A_{gal} varied from 0 to 40 with an interval size of $40/37 = 1.081$. The black line curve is for a sum of Poisson distributions, given by

Table 1. Results of fits to SPARC galaxy data for the galaxies shown using the graviton model (3), (4) and (5) with total baryonic mass $M_{bgal} = M_b(r_f)$ from (19). The items in the table from left to right are: 1) Galaxy, 2) Distance D, 3) Total Estimated Baryon Mass M_{bgal}, 4) Final Observed Rotation Velocity v_f, 5) Final Observed Orbital Radius r_f, 6) Maximum Observed Rotation Velocity v_{max}, 7) BTFR Normalization Multiplier A_{gal}, 8) GRST Coupling Scale Constant k, 9) GRST Coupling Exponent Constant β, 10) Disk Mass-to-Light Ratio Υ_{dsk}, 11) Fit Error Fit_{err}, and 12) Number of Observed Galaxy Points N_{obs}.

Galaxy	Dist	M_{bgal}	v_f	r_f	v_{max}	A_{gal}	k	β	Υ_{dsk}	Fit_{err}	N_{obs}
	(Mpc)	($M_\odot \times 10^{10}$)	(km·s^{-1})	(kpc)	(km·s^{-1})				($M_\odot L_\odot^{-1}$)	(km·s^{-1})	
CamB	3.36	0.002	16.8	1.47	16.8	7.162	1.92	−1.081	0.071	1.304	8
D631−7	7.72	0.057	57.3	7.19	58.5	1.069	2.16	−0.295	0.599	10.592	16
DDO064	6.8	0.07	46.9	2.98	46.9	2.923	0.88	1.868	1.787	9.819	14
DDO154	4.04	0.039	45.5	5.92	48.2	1.864	1.92	0.688	1.164	9	12
DDO161	7.5	0.304	66.1	13.37	67.5	3.188	1.04	−0.098	1.114	11.821	31
DDO168	4.25	0.097	52	4.12	55	2.659	0.88	0.688	1.857	15.849	10
DDO170	15.4	0.397	62.2	12.33	62.2	5.308	0.64	−0.098	3.398	14.799	8
ESO079-G014	28.7	9.357	178	16.67	178	1.864	0.16	−0.885	1.458	41.644	15
ESO116-G012	13	0.633	112	9.86	112	0.804	1.12	0.688	0.755	19.748	15
ESO444-G084	4.83	0.062	62.7	4.44	63.1	0.804	0.88	−0.491	5.409	10.644	7
ESO563-G021	60.8	38.126	312	42.41	321	0.804	0.32	−0.688	0.996	85.309	30
F561-1	66.4	0.196	50.4	9.66	50.4	6.102	2.96	4.426	0.008	12.422	6
F563-1	48.9	1.344	106	20.1	112.5	2.129	0.96	0.885	3.34	30.91	17
F563-V1	54	0.087	27.3	7.87	29.5	31.533	0.64	3.836	0.131	7.981	6
F563-V2	59.7	2.064	118	10.47	118	2.129	0.24	0.688	4.843	17.942	10
F565-V2	51.8	0.255	83.1	8.8	83.1	1.069	3.6	1.475	1.465	15.901	7
D512-2	15.2	0.081	35.9	3.83	37.2	9.811	0.24	0.295	2.107	7.471	4
D564-8	8.79	0.009	25	3.07	25	4.778	1.76	0.295	1.387	2.438	6
F567-2	79	0.462	52.2	9.59	52.2	12.46	0.24	2.655	1.362	12.787	5
F568-1	90.7	4.328	142	13.23	142	2.129	0.24	1.081	4.737	32.043	12
F568-3	82.4	3.58	120	17.98	120	3.453	0.32	−1.475	2.937	23.365	18
F568-V1	80.6	2.834	118	17.63	118	2.923	0.24	−1.475	5.12	25.69	15
F571-8	53.3	0.591	144	15.55	144	0.274	1.04	−0.491	0.49	46.558	13
F571-V1	80.1	0.593	83.9	13.59	84.3	2.394	1.12	0.688	1.483	15.524	7
F574-1	96.8	2.229	99.7	12.6	99.7	4.513	0.16	1.278	2.663	19.968	14
F574-2	89.1	0.342	40	10.83	40	26.765	0.24	3.049	0.429	6.761	5
F579-V1	89.5	0.679	114	15.16	114	0.804	3.76	2.262	0.206	30.156	14
F583-1	35.4	0.935	85.8	16.26	86.9	3.453	0.88	1.081	3.12	16.018	25
F583-4	53.3	0.443	69.9	7.29	69.9	3.718	0.4	−1.081	1.745	10.917	12
IC2574	3.91	0.248	67.5	10.23	67.5	2.394	4	1.868	0.533	12.509	34
IC4202	100.4	5.116	247	25.9	250	0.274	1.92	1.278	0.133	70.601	32

Continued

KK98-251	6.8	0.041	34.2	3.13	34.6	6.102	0.96	1.475	1.745	5.217	15
NGC0024	7.3	0.976	110	11.27	110	1.334	0.4	−1.278	2.061	21.912	29
NGC0055	2.11	0.744	86.5	13.5	87.4	2.659	1.2	1.278	0.538	11.887	21
NGC0100	13.5	0.461	91.2	9.62	91.2	1.334	0.96	−0.098	0.991	11.982	21
NGC0247	3.7	2.263	107	14.54	108	3.453	0.4	−1.278	2.235	16.294	26
NGC0289	20.8	8.872	165	71.12	194	2.394	0.24	0.491	0.575	55.592	28
NGC0300	2.08	0.712	93.5	11.8	97	1.864	0.64	−0.491	1.715	20.219	25
NGC0801	80.7	31.823	216	59.82	238	2.923	0.16	−1.475	0.735	60.785	13
NGC0891	9.91	5.051	208	17.11	234	0.539	0.32	0.098	0.266	63.867	18
NGC1003	11.4	1.398	115	30.24	115	1.599	1.12	0.491	0.597	38.72	36
NGC1090	37	3.504	160	30.09	176	1.069	1.12	1.278	0.199	38.595	24
NGC1705	5.73	0.105	71.5	6	73.2	0.804	0.48	−0.098	1.452	14.58	14
NGC2366	3.27	0.102	49.4	6.06	53.7	3.453	1.68	2.262	0.249	8.758	26
NGC2403	3.16	1.724	134	20.87	136	1.069	0.48	−0.098	0.929	30.599	73
NGC2683	9.81	4.846	151	34.62	212	1.864	0.24	0.295	0.552	49.642	11
NGC2841	14.1	30.06	294	63.64	323	0.804	0.32	−0.688	1.104	83.144	50
NGC2903	6.6	4.223	180	24.96	216	0.804	0.24	−0.098	0.442	48.641	34
NGC2915	4.06	0.151	86.5	10.04	86.5	0.539	1.12	0.491	0.902	32.937	30
NGC2955	97.9	21.234	227	35.43	276	1.599	0.16	0.491	0.456	78.808	24
NGC2976	3.58	0.283	85.3	2.27	88.7	1.069	0.32	−1.278	0.824	13.52	27
NGC2998	68.1	20.328	203	42.28	214	2.394	0.16	−0.491	0.976	64.112	13
NGC3109	1.33	0.164	67.3	6.45	67.3	1.599	1.68	0.098	4.503	9.909	25
NGC3198	13.8	3.288	149	44.08	157	1.334	1.28	1.081	0.242	33.172	43
NGC3521	7.7	4.86	206	17.74	220	0.539	0.32	−0.098	0.46	60.217	41
NGC3726	18	6.22	167	32.52	169	1.599	0.48	−1.278	0.676	41.381	12
NGC3741	3.21	0.037	51.6	7	51.6	1.069	1.44	0.098	3.208	13.985	21
NGC3769	18	1.519	113	37.16	126	1.864	0.64	0.491	0.348	26.054	12
NGC3877	18	4.362	169	11.35	171	1.069	0.4	2.065	0.433	56.558	13
NGC3893	18	4.159	167	19.05	194	1.069	0.32	0.295	0.52	35.044	10
NGC3917	18	4.216	137	14.86	138	2.394	0.24	−3.245	1.433	21.725	17
NGC3949	18	2.201	169	7.07	169	0.539	0.56	−0.491	0.465	32.343	7
NGC3953	18	14.257	215	15.68	224	1.334	0.08	0.098	0.787	40.282	8
NGC3972	18	2.578	134	8.72	134	1.599	0.24	−4.819	1.383	27.344	10
NGC3992	23.7	29.409	237	46.02	272	1.864	0.24	−0.885	1.114	52.818	9
NGC4010	18	1.184	122	10.47	129	1.069	1.12	0.885	0.458	27.43	12
NGC4013	18	5.572	170	31.01	198	1.334	0.56	−0.295	0.584	43.984	36
NGC4051	18	2.204	153	12.19	161	0.804	1.04	1.672	0.219	44.335	7

Continued

NGC4068	4.37	0.04	41.9	2.33	41.9	2.659	1.12	0.098	0.708	5.929	6
NGC4085	18	0.47	136	6.2	136	0.274	2.4	1.081	0.136	32.91	7
NGC4088	18	6.116	174	21.48	182	1.334	0.32	−1.081	0.418	35.444	12
NGC4100	18	5.111	159	22.76	195	1.599	0.32	0.491	0.717	49.573	24
NGC4138	18	2.036	150	18.58	195	0.804	0.48	0.491	0.369	41.404	7
NGC4157	18	6.264	185	29.61	201	1.069	0.4	−0.688	0.453	43.555	17
NGC4183	18	2.599	113	21.02	115	3.188	0.32	−1.278	1.636	22.51	23
NGC4214	2.87	0.113	80.6	5.63	80.6	0.539	0.72	−0.098	0.74	23.559	14
NGC4217	18	1.379	178	16.72	191	0.274	1.36	0.688	0.082	39.093	19
NGC4389	18	0.395	110	5.32	110	0.539	1.76	−0.098	0.137	21.766	6
NGC4559	9	1.338	119	20.97	124	1.334	4.56	3.442	0.013	26.811	32
NGC5005	16.9	6.778	265	11.47	265	0.274	0.32	0.491	0.299	56.823	18
NGC5033	15.7	5.937	196	44.59	225	0.804	0.24	0.295	0.324	55.001	22
NGC5055	9.9	8.158	172	54.59	206	1.864	0.24	0.098	0.392	34.84	28
NGC5371	39.7	27.365	213	46.24	242	2.659	0.08	−3.639	0.701	63.249	19
NGC5585	7.06	0.426	89.4	10.96	92.3	1.334	1.12	0.688	0.507	20.656	24
NGC5907	17.3	25.105	214	50.33	235	2.394	0.24	−1.475	1.097	48.27	19
NGC5985	39.7	52.76	285	34.72	305	1.599	0.08	−2.852	1.84	81.973	33
NGC6015	17	4.268	152	29.23	166	1.599	0.32	−0.295	0.986	45.324	44
NGC6195	127.8	24.436	246	36.43	258	1.334	0.16	−0.098	0.473	60.013	23
NGC6503	6.26	0.935	115	23.5	121	1.069	0.56	0.295	0.446	22.98	31
NGC6674	51.2	31.97	242	72.41	291	1.864	0.16	−1.081	1.25	57.428	15
NGC6789	3.52	0.018	60.4	0.71	60.4	0.274	1.52	−0.295	2.118	5.658	4
NGC6946	5.52	3.752	154	20.4	181	1.334	0.16	−0.098	0.436	38.965	58
NGC7331	14.7	12.909	238	36.31	257	0.804	0.32	−0.098	0.404	48.314	36
NGC7793	3.61	0.273	90.8	7.87	116	0.804	1.92	2.065	0.119	24.493	46
NGC7814	14.4	2.882	214	19.53	265	0.274	0.32	0.098	0.27	56.858	18
PGC51017	13.6	0.02	18.3	3.63	20.5	36.566	0.16	2.459	0.196	7.977	6
UGC00128	64.5	6.156	125	53.75	134	5.043	0.32	−0.688	3.61	27.673	22
UGC00191	17.1	0.853	83.85	9.98	83.85	3.453	0.32	−0.885	2.491	19.767	9
UGC00634	30.9	1.067	107.5	18.01	108	1.599	1.36	0.491	1.544	11.687	4
UGC00731	12.5	0.949	73.9	10.91	74	6.367	0.24	−0.098	14.977	9.541	12
UGC00891	10.2	0.153	63.75	7.39	63.75	1.864	1.6	0.098	1.662	9.026	5
UGC01230	53.7	4.328	103	36.54	113	7.692	0.16	−0.491	3.622	28.006	11
UGC01281	5.27	0.097	56.9	4.99	56.9	1.864	2.32	1.475	1.274	8.646	25
UGC02023	10.4	0.111	58.8	3.78	58.8	1.864	1.52	−0.885	0.665	5.956	5
UGC02259	10.5	0.959	90	8.14	90	2.923	0.24	−3.245	3.919	15.653	8

Continued

UGC02455	6.92	0.129	61	4.03	61	1.864	1.36	−1.278	0.115	7.879	8
UGC02487	69.1	65.761	333	80.38	383	1.069	0.4	−0.491	1.123	74.018	17
UGC02885	80.6	42.175	298	74.07	305	1.069	0.24	0.295	0.622	74.475	19
UGC02916	65.4	11.426	181	38	218	2.129	0.16	0.491	0.426	84.292	43
UGC02953	16.5	14.773	272	62.39	319	0.539	0.24	0.098	0.486	86.45	115
UGC03205	50	12.528	220	40.04	237	1.069	0.16	−0.688	0.87	65.84	48
UGC03546	28.7	3.744	193	29.23	262	0.539	0.32	0.098	0.282	75.31	30
UGC03580	20.7	0.951	124	27.06	131	0.804	1.36	0.688	0.124	34.165	47
UGC04278	9.51	0.593	92.8	6.69	92.8	1.599	0.96	0.098	2.004	23.603	25
UGC04305	3.45	0.132	33	5.52	37.3	22.261	0.08	3.836	0.394	13.867	22
UGC04325	9.6	1.024	91.5	5.59	92.7	2.923	0	−6	3.399	23.981	8
UGC04483	3.34	0.005	24.2	1.21	24.3	3.188	1.12	1.278	0.798	4.469	8
UGC04499	12.5	0.284	74.3	8.18	74.3	1.864	1.84	1.868	0.412	13.51	9
UGC05005	53.7	1.282	99.1	28.61	100	2.659	1.68	1.081	0.607	18.825	11
UGC05253	22.9	12.078	218	53.29	248	1.069	0.16	0.098	0.447	67.33	73
UGC05414	9.4	0.17	61.4	4.11	61.4	2.394	0.8	0.688	1.049	6.628	6
UGC05716	21.3	0.372	74.7	12.37	74.7	2.394	0.88	0.295	2.446	15.59	12
UGC05721	6.18	0.107	79.5	6.74	82.6	0.539	2.56	1.278	0.242	22.359	23
UGC05750	58.7	1.182	78.9	22.85	78.9	6.102	0.8	1.278	1.218	15.345	11
UGC05764	7.47	0.041	49.9	3.62	55.8	1.334	3.12	2.655	0.851	11.659	10
UGC05829	8.64	0.47	68.6	6.91	68.6	4.248	0.48	−1.475	4.227	7.684	11
UGC05918	7.66	0.187	44.5	4.46	44.5	9.546	0.08	−6	5.435	8.919	8
UGC05986	8.63	0.874	107	9.41	116	1.334	0.56	0.098	1.368	18.749	15
UGC05999	47.7	1.594	100	16.22	100	3.188	0.8	1.278	1.803	26.802	5
UGC06399	18	0.236	87.6	7.85	87.6	0.804	3.68	1.868	0.381	14.167	9
UGC06446	12	0.547	80.1	10.22	84.9	2.659	0.56	0.688	2.586	15.395	17
UGC06614	88.7	11.556	204	64.59	205	1.334	0.48	0.098	0.385	58.932	13
UGC06628	15.1	0.305	42.3	7.69	42.3	19.082	0.08	3.836	0.331	19.906	7
UGC06667	18	0.431	85.7	7.85	85.7	1.599	2.24	2.852	3.064	11.075	9
UGC06786	29.3	5.349	211	34.05	229	0.539	0.24	0.098	0.555	58.172	45
UGC06787	21.3	5.811	255	37.19	276	0.274	0.24	−0.098	0.397	68.234	71
UGC06818	18	0.123	74.4	6.98	74.4	0.804	4	0.688	0.267	19.287	8
UGC06917	18	1.012	111	10.47	111	1.334	1.2	1.475	0.773	16.611	11
UGC06923	18	0.231	81.1	5.16	81.1	1.069	1.44	1.475	0.363	18.508	6
UGC06930	18	2.709	108	16.61	109	3.983	0.24	−2.852	2.027	23.135	10

Continued

UGC06973	18	1.442	180	7.85	180	0.274	0.72	−0.491	0.213	32.679	9
UGC06983	18	1.128	109	15.68	113	1.599	0.96	1.081	0.931	23.509	17
UGC07089	18	0.624	79.1	9.16	79.1	3.188	0.64	−0.491	1.079	11.596	12
UGC07125	19.8	0.823	64.9	18.68	65.6	9.281	0.4	0.688	1.035	18.049	13
UGC07151	6.87	0.314	76.2	5.5	76.2	1.864	0.8	1.672	0.723	11.632	11
UGC07232	2.83	0.015	44	0.82	44	0.804	1.04	−1.672	1.063	5.541	4
UGC07261	13.1	0.401	76.1	6.67	76.1	2.394	0.48	−0.295	1.376	17.559	7
UGC07323	8	0.5	85.6	5.82	85.6	1.864	0.8	1.278	0.775	12.375	10
UGC07399	8.43	0.507	106	6.13	106	0.804	0.64	0.295	3.019	19.108	10
UGC07524	4.74	1.446	79	10.69	83.8	7.427	0.08	1.868	3.149	19.796	31
UGC07559	4.97	0.026	32.1	2.53	32.1	5.043	1.04	1.475	0.771	7.559	7
UGC07577	2.59	0.006	17.8	1.69	17.8	12.99	0.96	−3.639	0.587	2.384	9
UGC07603	4.7	0.067	64	4.11	64	0.804	1.36	0.295	0.944	8.77	12
UGC07608	8.21	0.153	69.3	4.78	69.3	1.334	1.84	1.278	3.037	11.66	8
UGC07690	8.11	0.103	55.9	4.13	60.7	2.129	0.56	1.278	0.598	11.753	7
UGC07866	4.57	0.035	33.1	2.32	33.1	5.837	0.48	−0.688	1.66	3.991	7
UGC08286	6.5	0.537	84.3	8.04	84.3	2.129	0.48	−0.885	2.901	17.892	17
UGC08490	4.65	0.289	77.6	10.15	80.1	1.599	0.48	0.098	1.638	15.896	30
UGC08550	6.7	0.13	57.5	5.36	57.8	2.394	0.56	−0.295	2.327	16.324	11
UGC08699	39.3	3.026	183	25.7	202	0.539	0.24	0.098	0.392	56.967	41
UGC08837	7.21	0.098	48	4.2	48	3.718	1.36	0.885	0.726	8.795	8
UGC09037	83.6	4.268	152	27.96	160	1.599	1.04	1.278	0.201	34.763	22
UGC09133	57.1	21.992	229	108.31	289	1.599	0.16	0.098	0.481	69.364	68
UGC09992	10.7	0.1	34.3	3.89	34.3	14.579	0	−6	1.661	6.448	5
UGC10310	15.2	0.723	73.2	7.74	73.2	5.043	0.16	−0.688	2.441	13.002	7
UGC11455	78.6	26.774	266	41.93	291	1.069	0.32	−0.098	0.593	65	36
UGC11557	24.2	0.812	84.5	10.56	85	3.188	0.56	0.885	0.351	22.536	12
UGC11820	18.1	0.743	84.45	15.82	84.45	2.923	0.56	−0.098	2.66	11.935	10
UGC11914	16.9	11.894	305	9.83	305	0.274	0.16	−1.475	0.78	74.401	65
UGC12506	100.6	37.468	225	49.99	255	2.923	0.16	−0.491	1.875	65.999	31
UGC12632	9.77	0.757	73.1	10.66	73.2	5.308	0.4	1.081	2.898	11.063	15
UGC12732	13.2	1.104	98	15.4	98	2.394	0.88	0.491	2.314	12.457	16
UGCA281	5.68	0.013	29.5	1.08	29.5	3.453	0.4	0.098	1.515	3.917	7
UGCA442	4.35	0.108	56.5	6.33	57.8	2.129	0.96	−0.098	4.048	8.362	8
UGCA444	0.98	0.048	38.3	2.62	38.3	4.513	0.48	−2.852	22.001	6.706	36

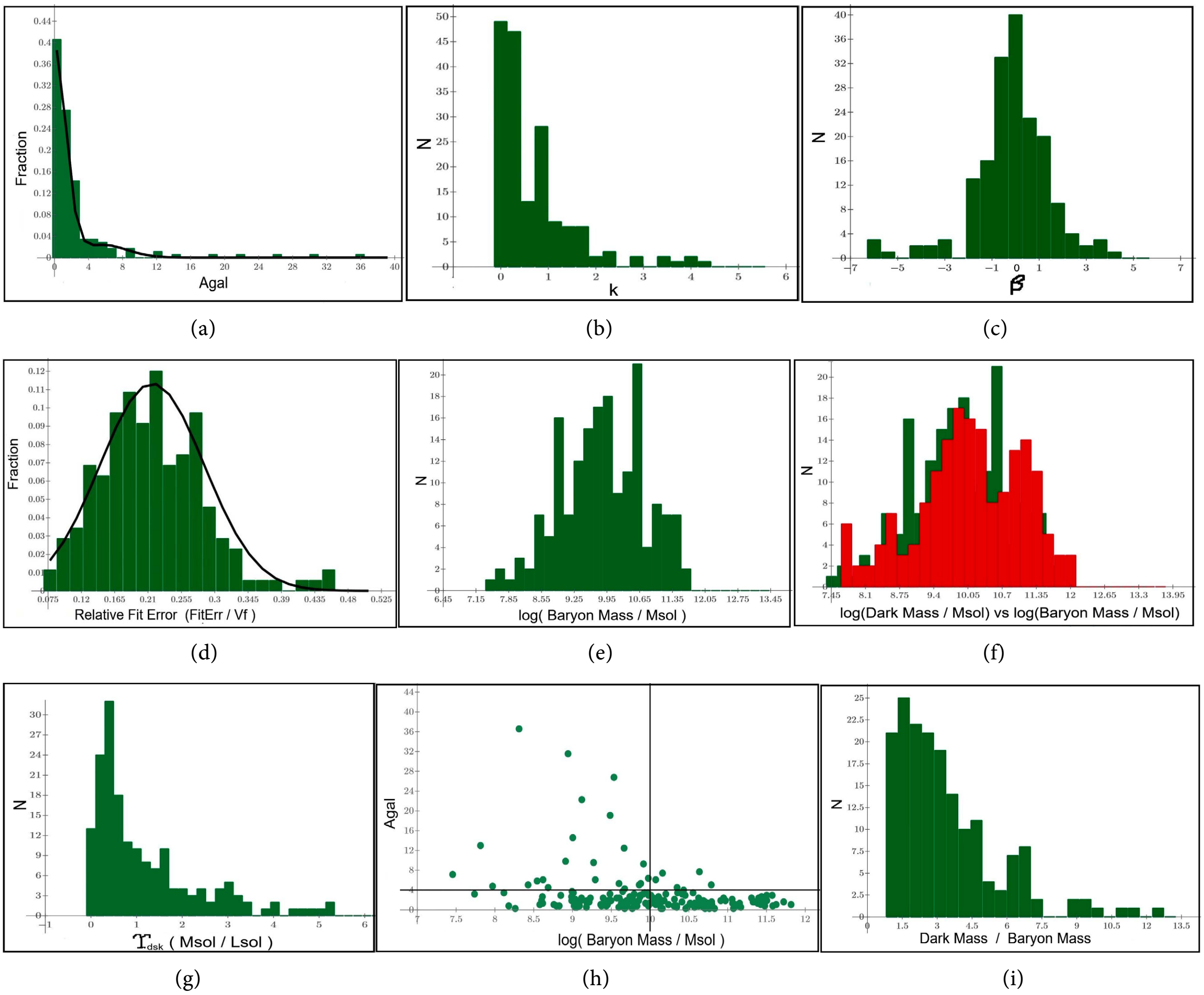

Figure 1. Fit parameters distributions. (a) BTFR Normalization multiplier. (b) GRST coupling scale constant. (c) GRST coupling exponent constant. (d) Relative fit error. (e) Total baryon mass. (f) Total dark mass vs. total baryon mass. (g) Mass-to-light ratio. (h) Baryon Mass vs. Agal. (i) Dark Mass/Baryon Mass.

$P_{sum} = (0.85)P(0.85, x) + (0.15)P(6.375, x)$, which is a rough fit to the distribution of the BTFR Normalization multiplier A_{gal} for the two classes of spiral galaxies, dwarf and regular, as shown in plot (h) of this figure, which is a plot of M_{bgal} vs. A_{gal} which shows 13.1% of $A_{gal} \geq 4$ and $M_{bgal} \leq 10^{10}\,\mathrm{M}_\odot$. Taking the first Poisson distribution $P(0.85, x)$, its mean is $\mu = 0.85$ and the standard deviation is $\sigma = \sqrt{\sigma^2 = \mu} = 0.92$.

Plot (b) shows the scale coupling constant k. This parameter is positive only and peaks at between 0 and 0.5, diminishing somewhat exponentially for higher positive values.

Plot (c) shows the exponent coupling constant β. This parameter is centered around 0 with approximately equal positive and negative values.

Plot (g) shows the mass-to-light ratio parameter Υ_{dsk} for the disk. The peak of the distribution is at approximately $0.4\,\mathrm{M}_\odot/\mathrm{L}_\odot$. The mass-to-light parameter for the bulge was defined by $\Upsilon_{bul} = 1.4\Upsilon_{dsk}$. The typical value assumed is $\Upsilon_* = 0.5\,\mathrm{M}_\odot/\mathrm{L}_\odot$.

3.2. Derived Parameters

Plot (d) shows the distribution of the relative fit error, which is the normalized velocity fit error for the galaxy over the final galaxy velocity, Fit_{err}/v_f, where $Fit_{err} = \sqrt{\left|\sum_{n=0}^{(N_{obs}-1)} v_{obs}^2(r_n) - v^2(r_n;k,\beta)\right|}$. This distribution is nicely approximated by a normal distribution with an average relative error of $\mu = 0.216$ and a standard relative deviation of $\sigma = 0.070$, which is described by the solid black curve in the plot. In this case, the normal distribution is normalized additionally by the factor $1/(2N_{fiterr})$ where $N_{fiterr} = 25$ is the number of divisions in the abscissa of relative fit error values.

Plot (e) shows the distribution of the galaxy total baryon mass.

Plot (f) shows the distribution of the galaxy dark mass (graviton gravitational redshift energy) overlayed on the galaxy baryon mass for comparison.

Plot (i) shows the ratios of dark mass to baryon mass for the galaxies.

3.3. Sample of Dwarf, Disk and Bulge Galaxies

In **Figure 2**, for a sample selected somewhat randomly, we present 15 of the 175 SPARC galaxies to which we made fits, that can be accessed at [5]. **Table 2** lists the presented galaxies showing the total baryon mass and the relative fit err (Fit_{err}/v_f). The average relative error for these 15 galaxies is 0.23, a somewhat large but respectable error considering that each fit to the rotation curve is based on the baryon mass distribution deduced from the measured bulge, disk and gas densities for each galaxy, which has its error bars. The average relative fit error for all of the 175 galaxies is 0.224. In the future, with higher resolution parameter sets, this error should be less.

3.4. Comparison with Other Dark Matter Methods

In **Figure 3** we show our fit for two galaxies, NGC 3109 and NGC 5055, which are also featured in [6] which compares two theories of dark matter halo processes, NFW (Navarro *et al.* [7]) and DC14 (Di Cintio *et al.* [8].) Both methods are similar in general with only minor differences, based on the dark matter density ρ_s defined by,

$$\rho_s(r;\alpha,\gamma,\omega) = \frac{M_{vir}}{4\pi r^3 (r/r_s)^\gamma f_s(c_{vir})\left[1+(r/r_s)^\alpha\right]^\omega}, \tag{23}$$

where M_{vir} is the virial mass, $f_s(c_{vir})$ is a function of the dark matter halo concentration and for NFW, $\alpha = \gamma = 1$ and $\omega = 2$ whilst for DC14, $\omega = (\beta_s - \gamma)/\alpha$ where α, β_s and γ are parameters related to the slope of the density profile. It was determined that the NFW method fits larger galaxies well such as NGC 5055 but is less capable for dwarf spirals such as NGC 3109. On the other hand, the DC14 method fits both galaxy types nicely by taking account of the relation of dark matter to baryonic mass in the galaxy.

Both of our fits to these galaxies are good with relative errors 0.15 for the dwarf spiral and 0.20 for the disk spiral. We show the similarity of the DC14 density ρ_s with our GRST density which, using (3), is given by,

$$\rho_{grst}\left(r;k,\beta\right)=\frac{M_b\left(r\right)}{4\pi r^3\left(r/r_f\right)^{\beta}\left[\left(3kr\int_0^r\left(M_b\left(s\right)/M_{bgal}s^2\right)\mathrm{d}s\right)^{-1}\right]}. \quad (24)$$

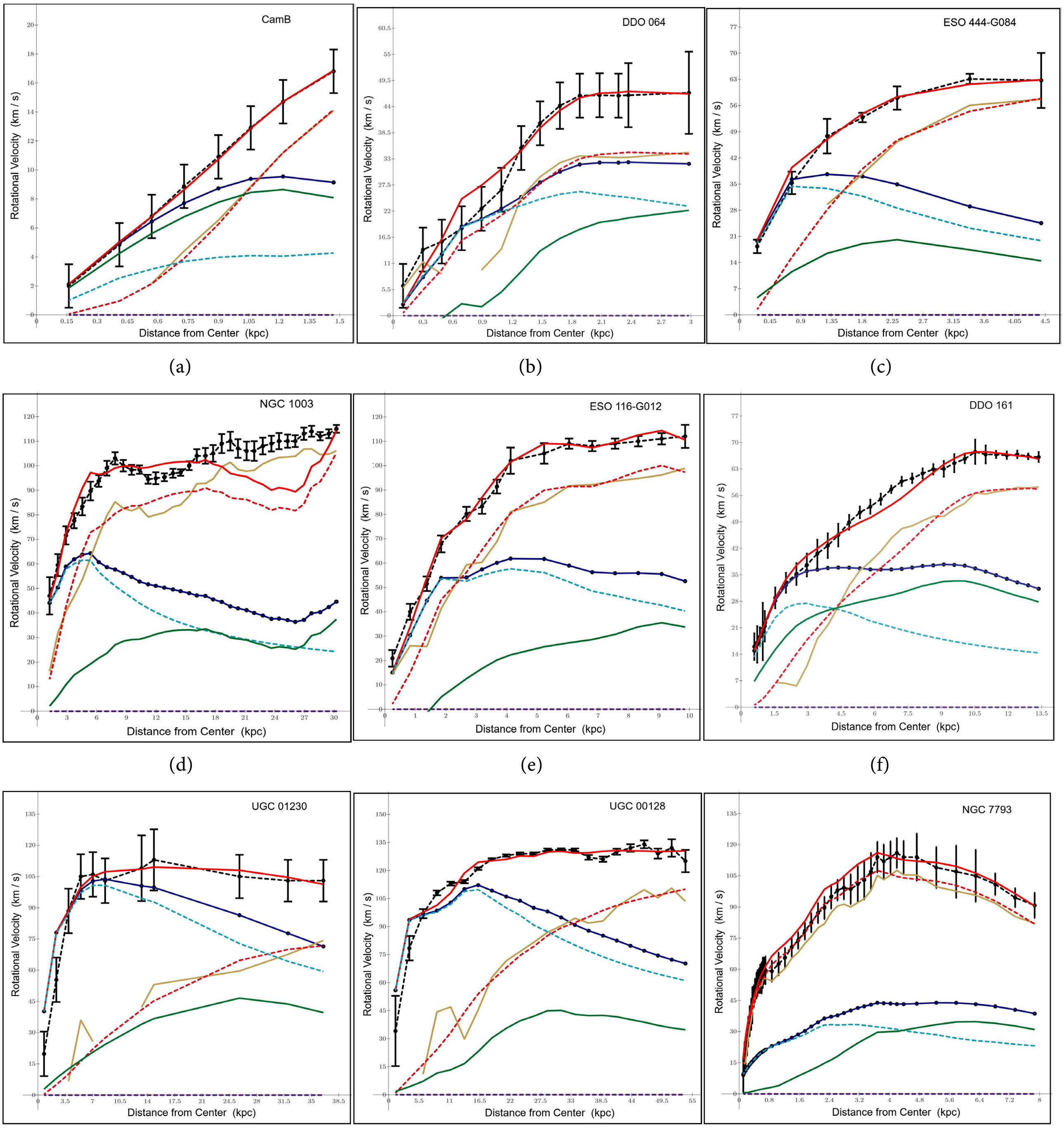

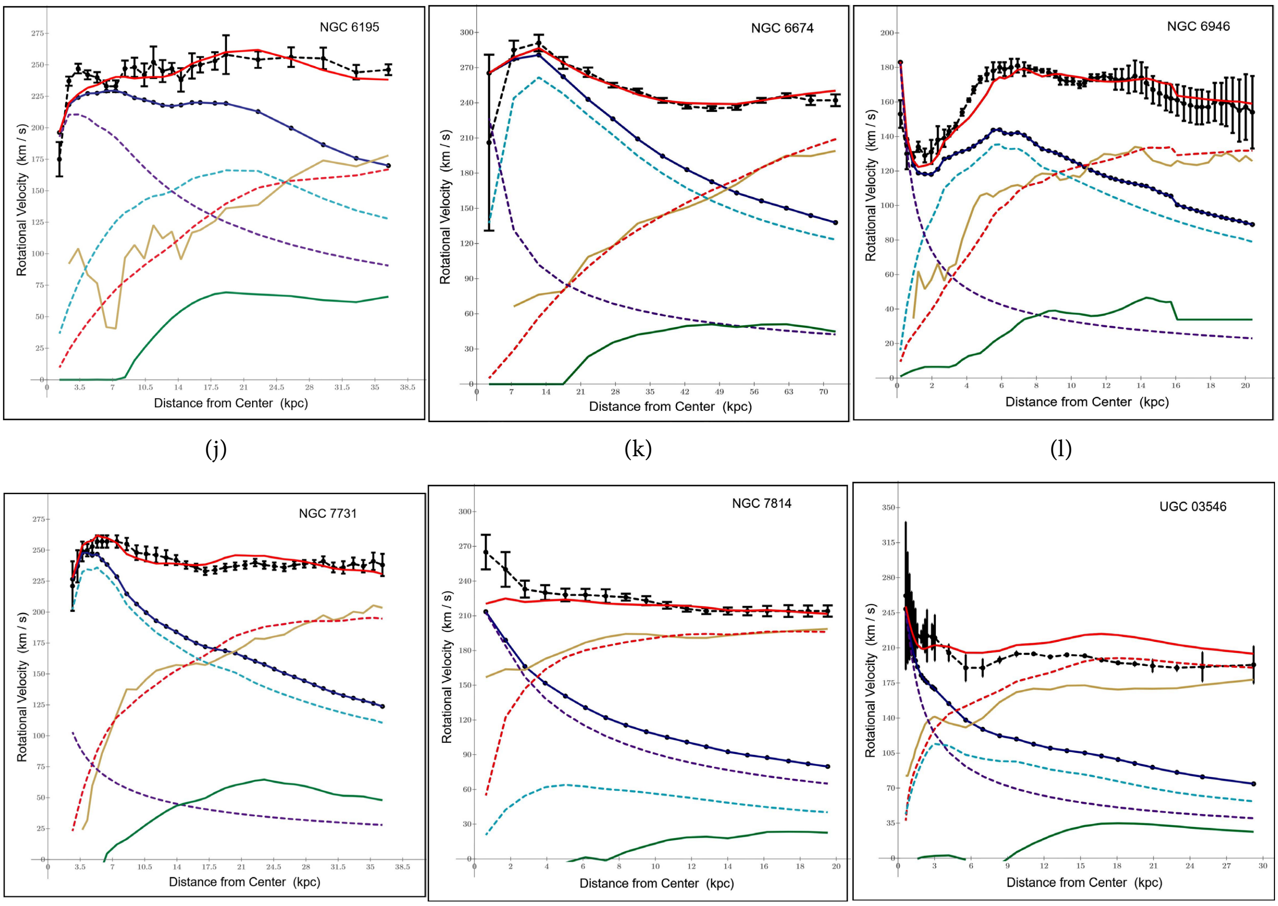

(j) (k) (l)

(m) (n) (o)

Figure 2. Sample galaxies. Dwarfs: CamB, DDO 064, ESO 444-G084. Disk Spirals: NGC 1003, ESO 116-G012, DDO 161, UGC 01230, UGC 00128, NGC 7793. Bulge and Disk Spirals: NGC 6195, NGC 6674, NGC 6946, NGC 7731, NGC 7814, UGC 03546. More details in Table 1 and Table 2.

Table 2. Brief summary for fits to sample galaxies in this paper.

Galaxy	M_{bgal}	Relative Fit Error
	($M_\odot \times 10^{10}$)	
Dwarf Spirals:		
CamB	0.002853	0.077
DDO 064	0.07073	0.21
ESO 444-G084	0.06218	0.17
Disk Spirals:		
NGC 1003	1.399	0.34
ESO 116-G012	0.6331	0.18
DDO 161	0.3044	0.18
UGC 01230	4.329	0.27
UGC 00128	6.156	0.22
NGC 7793	0.2735	0.27

Continued

Bulge and Disk Spirals:		
NGC 6195	24.44	0.24
NGC 6674	31.97	0.24
NGC 6946	3.753	0.25
NGC 7731	12.91	0.20
NGC 7814	2.883	0.27
UGC 03546	3.745	0.39

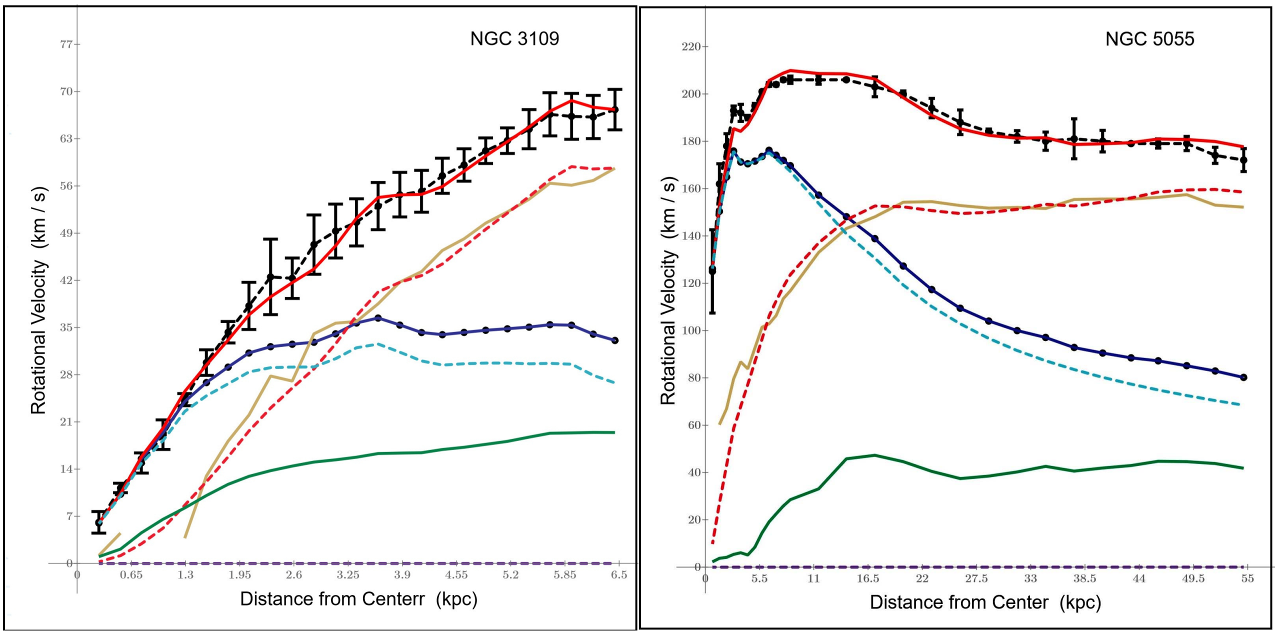

(a) (b)

Figure 3. Galaxies NGC 3109 and NGC 5055. NGC 3109 is a dwarf spiral with a determined galaxy baryon mass of $M_{bgal} = 1.641\times10^{9}\,M_{\odot}$, a disk mass-to-light ratio $\Upsilon_{dsk} = 4.503$ and relative fit error 0.15. NGC 5055 is a disk spiral with a determined galaxy baryon mass of $M_{bgal} = 8.158\times10^{10}\,M_{\odot}$, a disk mass-to-light ratio $\Upsilon_{dsk} = 0.392$ and relative fit error 0.20.

Equations (23) and (24) can be studied for equivalences, but this is beyond the scope of this report.

4. Conclusion

Upon the hypothesis that gravitons exist then they would be bosons of zero mass thus traveling in vacuum at the same speed as photons. Then, as for photons traveling against a gravitational field, the same kind of energy loss due to gravitational redshift would occur for gravitons. However, since gravitons and the gravitational field are one and the same then it is reasonable to hypothesize that the gravitational field will decrease in energy. It is this decrease in the field that the coupling factor $K(r;k,\beta)$ of (2) seeks to address. It is not unreasonable to assume that a more physical form for the coupling factor can be derived from first principles.

What the GRST offers is a connection of dark matter in the universe to baryons via gravitons.

The basic strategy of this study was to use a fixed set of parameters $\{(A_{gal,j}, k_j, \beta_j)\}$ as input to the GRST equation of motion (3) to fit any galaxy of the SPARC data base. The parameter set was determined after a single rough trial run through the 175 galaxies, where some fit failures were addressed by adjusting the input parameter set. The second run through all the SPARC galaxies is what this report describes. No further adjustments were made to make the fits. Any future pass through the data will be based on the fit parameters found already for each galaxy, searching in a vicinity thereof for a better fit to the galaxy rotation curve. Ultimately the quality of the fits depends on the accuracy of the stellar photometry and gas observations, which makes the GRST algorithm a possible tool for use in astrophysical observations since it can indicate where measurements may be excessive or lacking.

5. Data Availability

The author declares that the data supporting the findings of this study are available within the paper, its supplementary information files, and from the SPARC website http://astroweb.cwru.edu/SPARC/. Plots of all 175 fits to the SPARC galaxies are available in a compressed folder at
https://doi.org/10.13140/RG.2.2.17064.64008.

Conflicts of Interest

The author declares no conflicts of interest regarding the publication of this paper.

References

[1] Oliveira, F.J. (2026) Graviton Redshift Theory of Dark Matter in Spiral and Dwarf Galaxies. *Journal of High Energy Physics, Gravitation and Cosmology*, **12**, 252-266. https://doi.org/10.4236/jhepgc.2026.121016

[2] Lelli, F., McGaugh, S.S. and Schombert, J.M. (2016) SPARC: Mass Models for 175 Disk Galaxies with Spitzer Photometry and Accurate Rotation Curves. *The Astronomical Journal*, **152**, 157-170. https://doi.org/10.3847/0004-6256/152/6/157

[3] McGaugh, S.S. (2005) The Baryonic Tully-Fisher Relation of Galaxies with Extended Rotation Curves and the Stellar Mass of Rotating Galaxies. *The Astrophysical Journal*, **632**, 859-871. https://doi.org/10.1086/432968

[4] Lelli, F., McGaugh, S.S. and Schombert, J.M. (2016) The Small Scatter of the Baryonic Tully-Fisher Relation. *The Astrophysical Journal Letters*, **816**, L14-L19. https://doi.org/10.3847/2041-8205/816/1/l14

[5] Oliveira, F.J. (2026) Graviton Gravitational Redshift Fits to All 175 SPARC Galaxies. (Plots of All Galaxy Fits.) https://doi.org/10.13140/RG.2.2.17064.64008

[6] Katz, H., Lelli, F., McGaugh, S.S., Di Cintio, A., Brook, C.B. and Schombert, J.M. (2017) Testing Feedback-Modified Dark Matter Haloes with Galaxy Rotation Curves: Estimation of Halo Parameters and Consistency with ΛCDM Scaling Relations. *Monthly Notices of the Royal Astronomical Society*, **466**, 1648-1668. https://doi.org/10.1093/mnras/stw3101

[7] Navarro, J.F., Eke, V.R. and Frenk, C.S. (1996) The Cores of Dwarf Galaxy Haloes. *Monthly Notices of the Royal Astronomical Society*, **283**, L72-L78. https://doi.org/10.1093/mnras/283.3.l72

[8] Cintio, A.D., Brook, C.B., Dutton, A.A., Macciò, A.V., Stinson, G.S. and Knebe, A. (2014) A Mass-Dependent Density Profile for Dark Matter Haloes Including the Influence of Galaxy Formation. *Monthly Notices of the Royal Astronomical Society*, **441**, 2986-2995. https://doi.org/10.1093/mnras/stu729